NUMERICAL STUDY OF TWO-DIMENSIONAL HIGH-LIFT CONFIGURATIONS USING THE MSES CODE

Ana Lúcia Fernandes de Lima e Silva
Universidade Federal de Uberlândia – UFU
alfsilva@mecanica.ufu.br

João Alves de Oliveira Neto
Instituto de Aeronáutica e Espaço – Centro Técnico Aeroespacial
joaomanauara@yahoo.com

Alexandre Pequeno Antunes
Empresa Brasileira de Aeronáutica – Embraer
alexandre.antunes@embraer.com.br

Márcio Teixeira de Mendonça
Instituto de Aeronáutica e Espaço – Centro Técnico Aeroespacial
marcio_cta@yahoo.com

João Luiz F. Azevedo
Instituto de Aeronáutica e Espaço – Centro Técnico Aeroespacial
azevedo@iae.cta.br

Aristeu da Silveira Neto
Universidade Federal de Uberlândia – UFU
aristeus@mecanica.ufu.br

Abstract. *This work is inserted into the Embraer/FAPESP collaboration effort with universities and research centers to validate the capability of CFD codes to predict aerodynamic coefficients for high-lift configurations. This collaboration attempts to validate tools and methodologies to correctly predict aerodynamic coefficients using 2D and 3D codes. Numerical results are compared with experimental data for complex high-lift geometries at different flight conditions. At this first stage of the project, the 2D MSES code is evaluated using the NACA 0012 and the NLR 7301 geometries for Reynolds numbers of 2.51, 3, 6 and 9 million and Mach numbers up to 0.35. The ease of use and the capability to provide quick answers are very important in the early stages of design. MSES entirely fits in this initial design phase. The MSES code is a numerical airfoil design tool used to study single and multielement airfoils for a wide range of Mach and Reynolds numbers. It is based on the solution of the steady Euler equations by a finite volume discretization on an intrinsic streamlined grid. The boundary layers and trailing wakes are described by a 2-equation integral formulation with lagged dissipation closure. The inviscid and viscous regions are coupled via the boundary layer displacement thickness. The overall system is solved using a Newton method. The results of drag, lift, momentum and pressure coefficients are presented for the single and multielement airfoil mentioned above. The present calculations are compared with the data available in the literature for both airfoils.*

Keywords*: high lift, aerodynamic forces, MSES code, 2D simulations*

1. Introduction

In the early stages of the preliminary design of an airplane, some of the aerodynamic coefficients are already know due to a certain airplane performance that has to be achieved. In particular, the high-lift devices are intrinsically connected with the landing and the take-off performance. This two phases of the airplane mission are very important due to the operational implications that they have. An overestimated take-off Cl maximum implicates in limitations in the maximum weight to take-off, or the need for an longer track. In the same way, an overestimated landing Cl maximum implicates in the necessity for a longer track. These facts generate the unavailability to operates in some airports, and as consequence, the airplane might not be convenient for some airliners.

The Embraer/FAPESP collaboration has the main objective to minimize at most, all the uncertainties associates in process of designing high-lift devices. The high-lift configurations are usually complex geometries, and at which, complex flow physics are presented. This collaborations has the objective of evaluate not only the numerical tools used in the high-lift design configurations, but also to obtain the most indicated methodology to achieve the design goals.

Computational Fluid Dynamics (CFD) has been exhaustively used for aerodynamic design purposes due to the constant increase of the computational capabilities, the development and improvement of methodologies and the ease to

obtain reliable results. Most numerical codes for aerodynamic design are based on the solution of the Navier-Stokes equations or the Euler/boundary layer coupled equations such as the MSES code (Drela, 1996), used for this study.

The prediction of high lift configurations is a challenge due to the complexity of the flow physics. One can mention the flow separation, the boundary layer transition to turbulence and also the interaction between the wakes formed by each element of the configuration.

The present paper uses the MSES code (Drela, 1996) to simulate flows around aerodynamic configurations aiming at the prediction of drag, lift and momentum coefficients to evaluate how MSES is inserted in the main objective of this collaboration, and which consists in getting the aerodynamic coefficients as real as possible. The numerical results for the NACA 0012 and the NLR 7301 configurations are presented together with numerical and experimental results from the literature.

2. Mathematical Formulation of MSES

The MSES code is a two dimensional analysis, design and optimization framework for multi-element airfoil sections. It is based on the steady state conservative Euler equations:

Conservation of mass

$$\oint r\vec{q}.\vec{n}ds = 0 \tag{1}$$

Conservation of momentum

$$\oint \left(r\left(\vec{q}.\vec{n}\right)\vec{q} + p\vec{n}\right)ds = 0 \tag{2}$$

Conservation of energy

$$\oint r\vec{q}.\vec{n}h_t ds = 0 \tag{3}$$

where r is the fluid density, $\vec{q}$ is the velocity vector, $\vec{n}$ is the normal vector, p is the pressure and h_t the stagnation enthalpy.

The Euler equations are used to describe the inviscid part of the flow. The assumption that the viscous part is restricted to a thin boundary layer and wake is made, and the viscous part is described with the boundary layer theory given by the integrated Prandtl boundary layer equations (White, 1991). The momentum and energy integral relations used by the MSES program have the following form

$$\frac{dq}{dx} + \left(H + 2 - M_e^2\right)\frac{q}{u_e}\frac{du_e}{dx} = \frac{C_f}{2} \text{ , and} \tag{4}$$

$$q\frac{dH^*}{dx} + \left(2H^{**} + H^*\left(1-H\right)\right)\frac{q}{u_e}\frac{du_e}{dx} = 2C_D - H^*\frac{C_f}{2}, \tag{5}$$

where q is the momentum loss thickness, $H = d^*/q$, $H^* = q^*/q$ and $H^{**} = d^{**}/q$ are shape factors and d^* and d^{**} is the displacement thickness and density thickness, respectively. The u_e and M_e terms are the velocity and the Mach number at the edge of the boundary layer, x is the streamwise coordinate, C_f and C_D are the friction and the dissipation coefficients, respectively. These equations are valid for both laminar and turbulent boundary layers and also for wakes. For the calculation of the closure relations, C_f, C_D, H^* and H^{**}, a distinction is made for laminar and turbulent boundary layers. The solution of the boundary layer equations is coupled to the inviscid solution through the boundary layer edge, where the inviscid computations are used as boundary conditions for the boundary layer and the boundary layer solution is used to modify the inviscid computation.

The equations are discretized in an intrinsic grid, where one set of coordinate lines correspond to the streamlines around the body. With this procedure the number of unknowns per grid node is reduced from four to two because the continuity equation and the energy equation can be replaced by the simple condition of constant mass flux and constant stagnation enthalpy along each streamtube. The Newton method is used for solving the system of nonlinear equations. More detailed information about the MSES code can be found in MSES user's guide (Drela, 1996).

3. MSES Framework

MSES is an integrated workbench were one can find a mesh generator, a solver code, an inverse design code, and a post-processing software. This integrated workbench is a friendly environment where the mainly input is a file with the coordinates of the geometry of interest. The Fig. 1 shows an overview of the software system that composes this workbench environment.

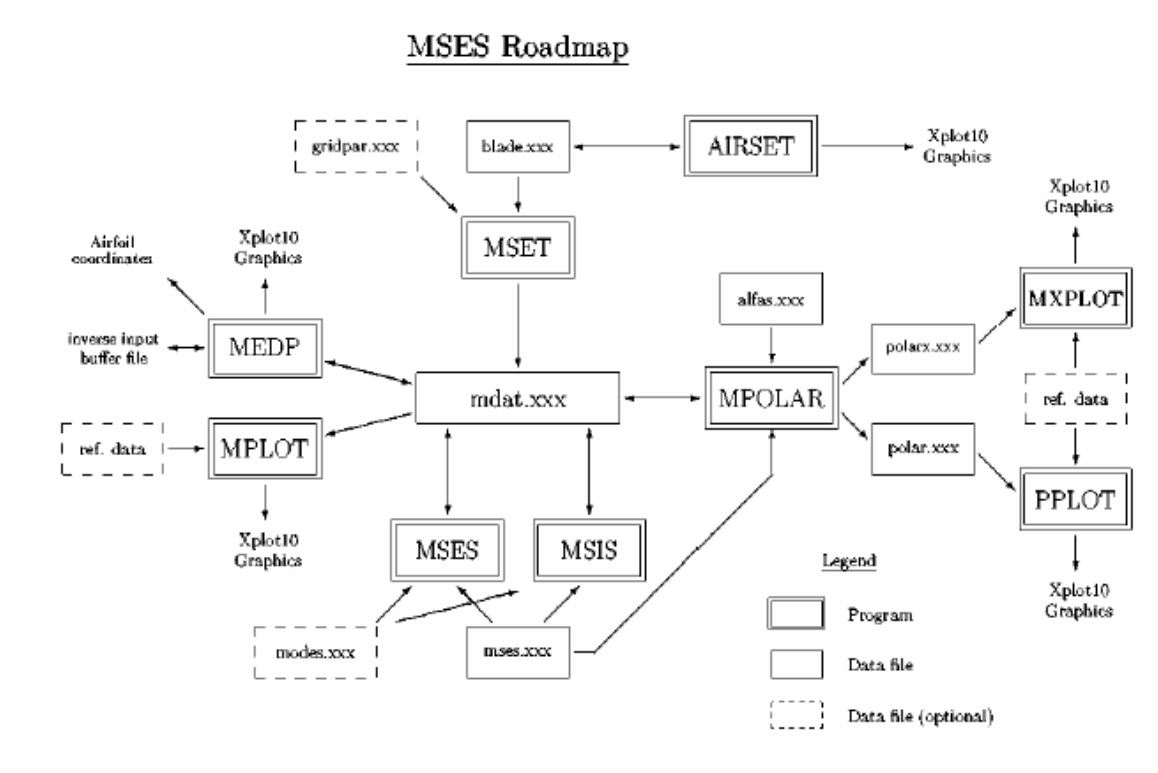

Figure 1. MSES workbench environment.

4. Numerical Results

The simulations are carried out for Reynolds numbers of 2.51, 3, 6 and 9 million and for Mach number (M_∞) up to 0.35. The results of drag, lift and momentum coefficient are presented and compared with experimental results available on the literature.

4.1. Results for the NACA 0012 Airfoil

The NACA 0012 is a symmetric, single element airfoil with a relative thickness of 12%. Simulations are performed with this profile for Reynolds number of 3, 6 and 9 million, at Mach number of 0.17 and 0.30 . These results were compared with the experimental results (Abbott and Von Doenhoff, 1959) for M_∞ = 0.17, and with the experimental results (Seifert and LaTunia, 1999) for M_∞ = 0.3 .

For the numerical and the experimental results, the lift coefficient as a function of the angle of attack can be observed in Fig. 2(a). The MSES results are very close to the experimental in the linear region of the curve. This good agreement is obtained up to α = 14 deg. Beyond this angle of attack, the non-linear viscous affects are more relevant, and MSES looses the ability to capture with accuracy the stall angle of attack and Cl maximum. At Re = 3.0 x 10^6 the angle of maximum lift obtained by MSES was 17 deg., which is in accordance with the experimental results. Therefore, Cl maximum obtained by MSES, Cl maximum=1.6, is approximately 7% higher than the experimental value, Cl maximum=1.7. At Re = 6.0 x 10^6 the stall angle predicted with MSES is α = 18 deg. with Cl maximum= 1.7. For the experimental data, the stall angle is α = 16.5 deg. and Cl maximum experimental at 1.6 .

Figure 2(b) presents the numerical results of Cd as a function of Cl, compared with the experimental results for the three Reynolds numbers of interest. The MSES Cd results were higher than the experimental line up to Cl approximately equal to 0.9, and lower than the experimental line after this value. Part of these discrepancies in the drag coefficient is due to the difference in Cl value between the experimental and the numerical results, for a given angle of attack. Because the numerical calculations present a higher Cl value, one should expected to have a higher Cd value. This assertive is based on the fact that, as Cl increases, the boundary layer is more stressed due to the adverse pressure

gradient after a highly negative Cp peak on the leading edge of the airfoil. This stress leads to an increase in the boundary layer thickness, and as consequence an increase in the drag component associated with the pressure. One can also observe that airfoil stall for the numerical calculations is postponed in relation to the experimental data. Therefore, one can expect that the divergence in the drag coefficient for the numerical results should begin at a higher alpha, or at a higher Cl value. This observation explains the lower growth rate in the Cd coefficient for the numerical results in relation to the experimental results after a Cl value of 0.9.

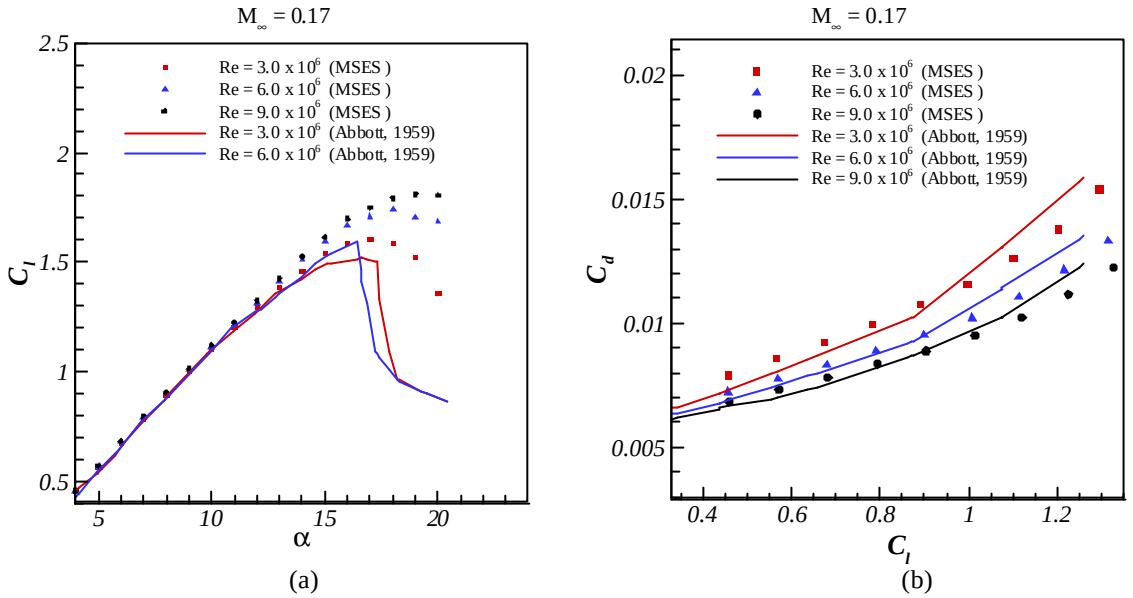

Figure 2 (a). Lift coefficient as a function of angle of attack ; and (b) drag coefficient as a function of Lift coefficient (b). Symbols are the MSES results and lines are the experimental results of Abbott (1959).

The drag coefficient results obtained with MSES for M_∞ = 0.3 are presented in Fig. 3 together with the experimental results (Seifert and LaTunia, 1999). A very good agreement can be observed up to a = 12 deg. For an angle of attack higher than 14 deg., the experimental results presents an rapid increase in the drag coefficient, which is a typical behavior from a boundary layer detachment. The numerical calculation shows an increase in drag coefficient as well, although not so intense as the experimental data. This increase in the drag coefficient, of the numerical result, is associated with boundary layer thickening and a detached flow region around 85% of the chord. This flow separation begins around alpha of 14 deg. and, as the angle of attack increases, the detached region moves in direction to the leading edge of the airfoil.

One can observe in Fig. 4 the shape factor curve. The shape factor H is defined as the ratio between the displacement thickness, d^*, and the momentum thickness, q . This coefficient is an important parameter to check de boundary layer detachment. Usually, for an turbulent boundary layers over a flat plate, whenever the shape factor is higher than 2.4, one can observe flow separation (Cebeci and Bradshaw, 1977). Figure 4 represents the shape factor for the profile at an angle of attack of 14 deg., and using the shape factor criteria the detached region is supposed to start at 80% of the profile chord. Therefore, it makes sense to observe the beginning of a detached region around 85% of the profile chord.

One can observe in Fig. 5 that MSES results show reasonable agreement with the experimental data (Abbott and Von Doenhoff, 1996) up to a = 11 deg. For angles higher than 11 deg. there are discrepancies between the numerical and the experimental results. It is well known that, Cm coefficient is very sensitive to small discrepancies in the Cp distribution. The smallest difference in Cp can provoke an different Cm coefficient. At higher angle of attack this tendency is stronger than in lower angle of attack as one can observe in Fig 5.

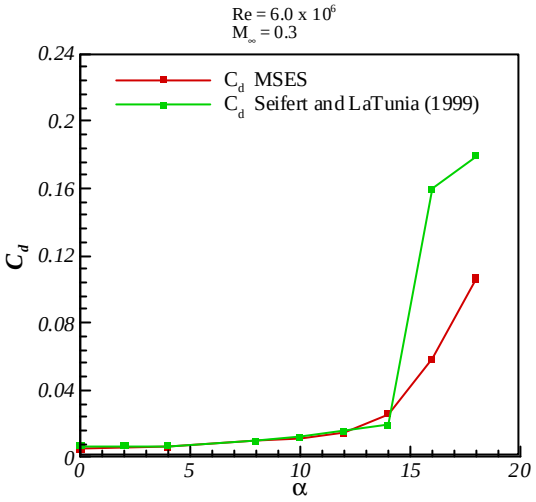

Figure 3. Drag coefficient as a function of angle of attack. Red line indicates the MSES results and green line is the experimental data (Seifert and LaTunia, 1999).

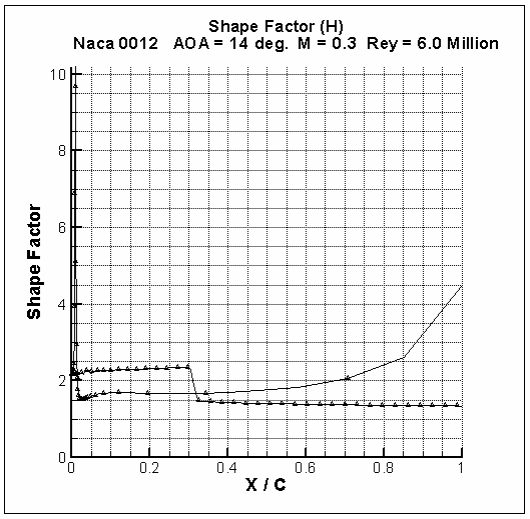

Figure 4. Shape factor, *H*, for alpha of 14 deg.

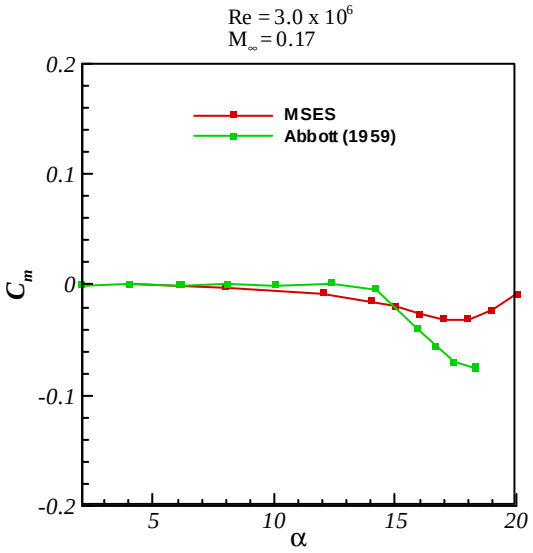

Figure 5. Momentum coefficient as a function of the angle of attack. Cm compared with the experimental results (Abbott and Von Doenhoff, 1959).

4.2. Results for the NLR 7301 Airfoil

The NLR 7301 geometry is composed by a main element and a flap device. In this study, two different configurations are evaluated. The first analysis is performed for the configuration with a flap gap of 1.3%, and the second one with a flap gap of 2.6%. The gap is defined as the radius of the circumference centered in the trailing edge of the main element and tangent to the flap profile in a certain point. This point of tangency is defined by the overlap, which is held at a constant at a value of 5.3% for both test cases here considered. Figure 6 shows the geometrical definition of the gap and the overlap. It worth to mention that the gap and the overlap are defined as a percentage of the nominal profile cruise chord.

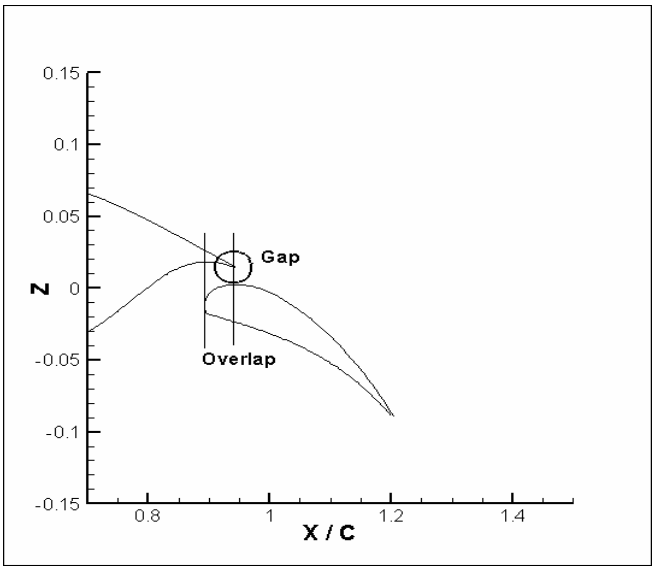

Figure 6. Gap and overlap definition.

The experimental results are available (Van der Berg and Gooden, 1994). The numerical Cp distribution shows an excellent agreement with the experimental data for the evaluated angles of attack, except in the cove region. Figure 7 show, for both flap gaps at an angle of attack of 6 deg., the comparison between the numerical and the experimental Cp distributions. In Fig. 8, one can observe the comparison for an angle of attack of 10.1 deg. In Fig. 9, one can observe the difference in the Cp distributions in the region of the cove. This difference leads to a higher Cl value, as it is shown in the Cl versus α curve.

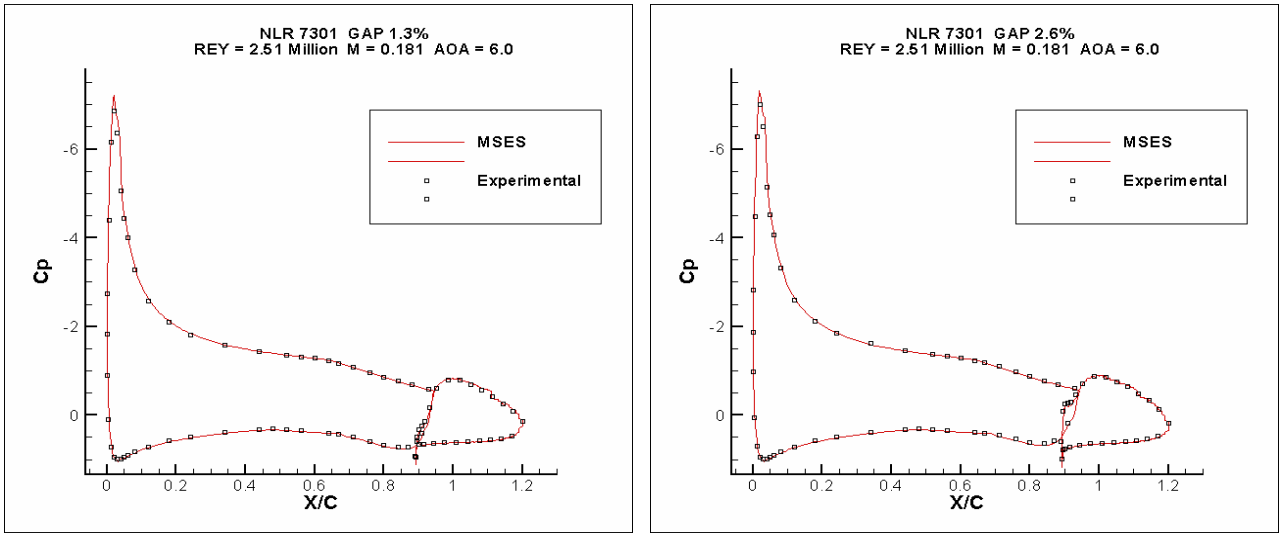

Figure 7. Cp distribution comparison for 6 deg. angle of attack with 1.3% gap (left) and 2.6% gap (right).

In Fig. 10, one can observe the comparison for the Cl versus α curve. As in the NACA 0012 airfoil study the MSES results also present an overprediction of Cl for this geometry. Due to the complexity of this simulated geometry, the differences in the Cl versus α curve seem to have been more accentuated. For an perfect match with the experimental results, all the complex physics has to be perfectly capture. This includes the flow features at the cove of the main element, as well as the interactions between the free shear layer of the main element and the boundary layer of the flap.

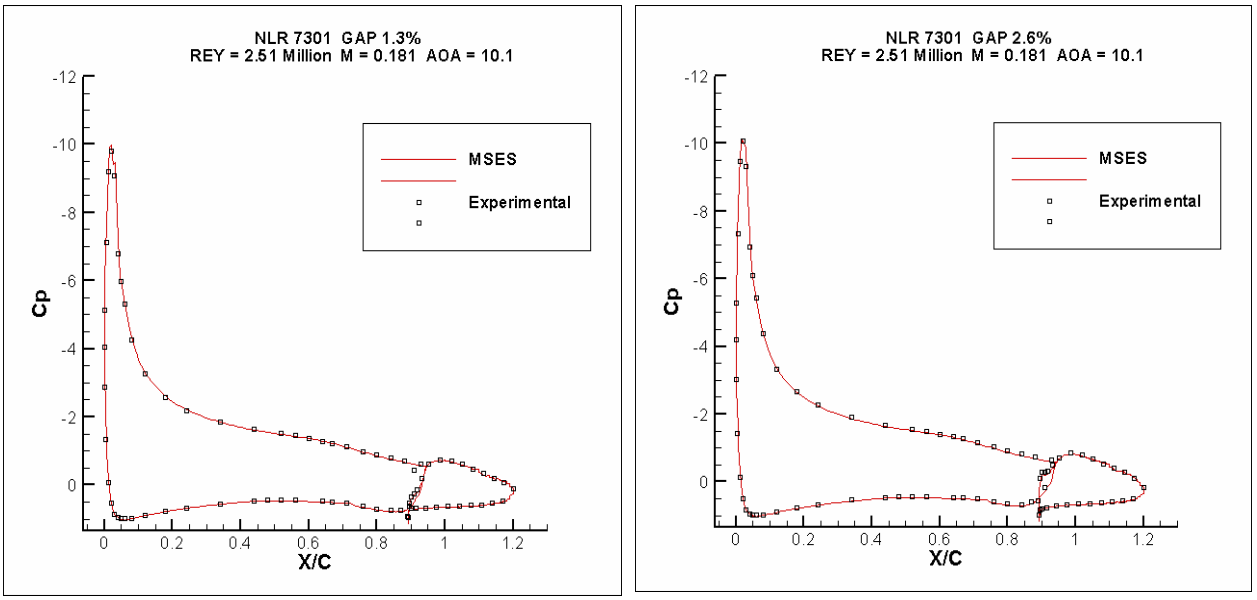

Figure 8. Comparison of Cp distributions for angle of attack of 10.1 deg.

MSES code show a good capability to effectively reproduce the experimental data at the linear range. The limitations presented in the non-linear region are intrinsic to the MSES formulation, as well the lack of a better control in relation to the mesh generation. This verification does not take the merits of the code since even other numerical codes with an formulation more adequate, Navier-Stokes with an turbulence model, presents the same difficulty to present the aerodynamic coefficients with accuracy.

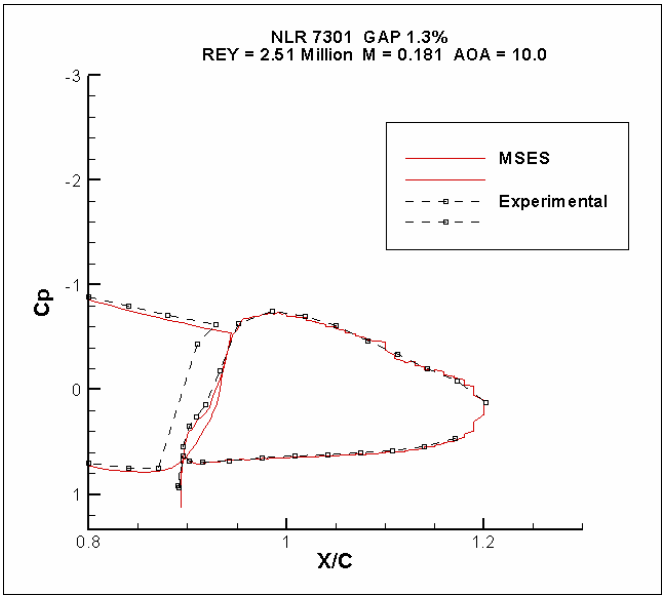

Figure 9. Cp differences in the cove region.

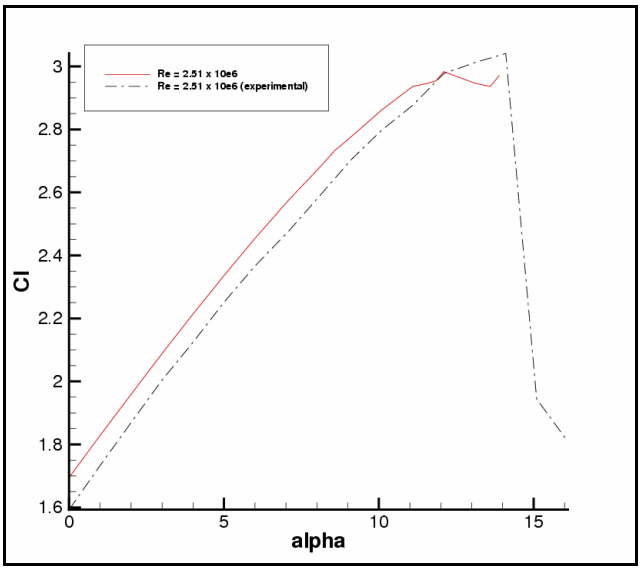

Figure 10. Cl versus α curve for the numerical and the experimental results for the NACA 0012 airfoil.

5. Conclusions

For the NACA 0012 airfoil, the lift computational results are very close to the experimental data (Abbott and Von Doenhoff, 1959) up to 14 deg. At this angle of attack, the results at Reynolds number of 3 million are in better agreement than the results at Reynolds number of 6 million. Near the stall, MSES code looses the ability to perfectly match the experimental results. The same behavior is observe in the drag coefficient curve. In the comparison with the experimental results (Seifert and LaTunia, 1999), with the experimental data good agreement is achieved up to a = 12 deg. Beyond this angle of attack, MSES results do not agree very well, and the drag rise is more conservative than the experimentally observed one. The same type of behavior is observed for the Cm curves. In the linear region of the curve, an reasonable agreement can be observed. However, for higher values of the angle of attack, discrepancies become evident. For the NLR 7301 geometry, the same tendencies are observable in general except that the discrepancies are more pronounced due to the geometrical complexity of the configuration.

The MSES code, in general terms, presented certain discrepancies with the experimental results in regions where the non-linearities govern the flow behavior. Therefore, in a preliminary design phase, in which changes are implemented every day, MSES is an adequate tool due to the ease of operation and the low cost of the calculations. Furthermore, the MSES code is completely capable indicating aerodynamic differences between two different geometries and it gives an indication of which one is recommended due to its better aerodynamic behavior. For this reason, MSES is an very helpful tool in the early stages of aerodynamic design.

6. Acknowledgements

The authors would like to acknowledge Embraer (Empresa Brasileira de Aeronáutica) for the support provided for this work. The authors also acknowledge the support of Fundação de Amparo à Pesquisa do Estado de São Paulo, FAPESP, through the Research Grant No. 2000/13768-4.

7. References

Abbott, I. H. and Von Doenhoff, A. E., 1959, “Theory of Wing Sections”, Dove.

Cebeci,T. and Bradshaw, P., 1977, “Momentum Transfer In Boundary Layers”, Hemisphere Publishing Corporation.

Drela, M., 1996, “A User's Guide to MSES 2.92,” MIT Computational Aerospace Sciences Laboratory.

Seifert, A. and LaTunia, G. P., 1999, “Oscillatory Excitation of Unsteady Compressible Flows over Airfoils at Flight Reynolds Numbers”, AIAA 99-0925, Vol. 13, pp. 1-15.

Van der Berg, B. and Gooden, J., 1994, “Low-Speed Surface Pressure and Boundary Layer Measurement Data for the NLR 7301 Airfoil Section with Trailing Edge Flap”, A Selection of Experimental Test Cases for the Validation of CFD codes, AGARD AR – 303, Vol. II, pp. A2-A9.

White, F. M., “Viscous Fluid Flow”, 1991, McGraw-Hill International Editions, second edition.

8. Responsibility notice

The authors are the only responsible for the printed material included in this paper.